Electronic structure as a guide in screening for potential thermoelectrics: Demonstration for half-Heusler compounds

Zhenzhen Feng, Yuhao Fu, Aditya Putatunda, Yongsheng Zhang, and David J. Singh

Phys. Rev. B **100**, 085202 — Published 12 August 2019

DOI: 10.1103/PhysRevB.100.085202

Electronic Structure as a Guide in Screening for Potential Thermoelectrics: Demonstration for Half-Heusler Compounds

Zhenzhen Feng,[1,2,3] Yuhao Fu,[3] Aditya Putatunda,[3] Yongsheng Zhang,[1,2,*] and David J. Singh[3,4,†]

[1] *Key Laboratory of Materials Physics, Institute of Solid State Physics, Chinese Academy of Sciences, Hefei 230031, China*

[2] *Science Island Branch of Graduate School, University of Science and Technology of China, Hefei 230026, China*

[3] *Department of Physics and Astronomy, University of Missouri, Columbia, MO 65211-7010, USA*

[4] *Department of Chemistry, University of Missouri, Columbia, MO 65211, USA*[‡]

(Dated: July 26, 2019)

We adopt a high throughput search strategy that begins with electronic structure features to screen a set of half-Heusler compounds for thermoelectric performance. This is motivated by the contradictory electrical transport requirements, specifically high electrical conductivity, σ and high thermopower, S, for obtaining high figure of merit, ZT. We use an electronic fitness function that measures the extent to which a specific band structure decouples σ and S for this purpose. We then perform detailed, more costly, calculations of thermal conductivity and electrical properties for those compounds that have a high electronic fitness. This provides an efficient method for identifying promising compounds from a set of candidates. We apply this to a set of 75 previously studied half-Heusler compounds. The approach identifies several compounds as having potential as thermoelectric materials. Importantly, these include not only some previously identified candidates, but also some other compounds that had not been identified previously using other screening methods.

I. INTRODUCTION

Thermoelectrics is a subject of renewed interest in part due to the possible uses in energy technology and also in large part because of the fascinating science that underlies high thermoelectric performance.[1–5] This science is associated with the contradictory combination of transport coefficients needed for thermoelectric performance. This is thought to underlie connnections of thermoelectricity with exciting topics such as topological materials (e.g. Bi_2Te_3),[6–9] quantum criticality (e.g. $BaFe_4Sb_{12}$, Na_xCoO_2),[10–13] superconductivity (SnTe, GeTe),[14] and ferroelectricity (GeTe).[15]

Besides the diverse and often subtle physics underlying thermoelectricity, the realization of high performance in any given material generally requires extensive optimization. This complicates experimental searches for high performance thermoelectrics. It also provides an important role for theory both in the identification of promising thermoelectric compounds and in guiding their optimization,[1,4,16,17] as well as in elucidating the underlying physics. An implication is that thermoelectricity is a particularly rich area for testing and demonstrating theory based materials search strategies.[18–22] Here we report and demonstrate a high throughput strategy that starts with a simple electronic structure based metric. Application to a set of half-Heusler compounds identifies previously known high performance materials. Importantly, this approach also identifies additional promising compositions, underscoring the importance of electronic structure in thermoelectric performance.

The energy conversion efficiency of thermoelectric devices is limited by the thermoelectric figure of merit of the materials used. This is given by $ZT = S^2T\sigma/(\kappa_e + \kappa_l)$, where S is the Seebeck coefficient, σ is the electrical conductivity, κ_e is the electronic thermal conductivity, κ_l is the lattice thermal conductivity, and T is the absolute temperature.[1] The electrical terms in the numerator are termed the power factor, $PF = \sigma S^2$. It is important to note that σ and S have strong dependence on both doping level and temperature, and that they are counter-correlated.

This goes beyond the well-known and frequently discussed fact that, within single parabolic band (SPB) models that are popular in analysis of thermoelectric data, the Seebeck coefficient decreases with carrier concentration while the conductivity increases resulting in an optimum carrier concentration for peak PF.[23] In particular, it suggests the use of materials that do not follow the SPB in order to weaken the SPB counter-correlation between σ and S. This is facilitated by the modern ability to calculate band structures from first principles, as well as transport tools that allow one to quantify the impact of arbitrary band structures on transport quantities. This leads then to an important area of thermoelectrics research, which is the identification and exploitation of unusual band structure features to decouple the normally counter-correlated electrical transport properties and enable high ZT.[4,24–34]

High throughput methods are an important recent development in the search for new materials.[35] These depend on effective quantitative metrics that can be used in identifying materials and which can be efficiently and reliably obtained from calculations. Here we explore the use of a function that characterizes the decoupling of σ and S afforded by a given band structure in this context.[36–38] The approach emphasizes the importance of band structure by using it as a first screen. This allows us to find materials that exhibit features that are identified with high thermoelectric performance without relying on qualitative considerations that are difficult to implement in high throughput searches.

We apply this to a set of half-Heusler compounds. This class of compounds includes many materials with mechanical robustness and thermal stability, and in addition is the basis of a number of known high performance thermoelectrics.[20,39–45] It is a large class of materials, and many possible compounds remain largely unexplored.[46] In addition, the study of half-Heusler compounds for thermoelectrics is complicated by polytypism that occurs with many compounds. For example, LiZnSb was reported as an excellent thermoelectric in its hexagonal structure, but was also found in a half-Heusler polytype, which is the ground state; TaFeSb is a material that was predicted and was only recently synthesized as a high performance thermoelectric;[45] and CoVSn, which was variously predicted to be stable or not stable,[20,27,47] has been reported as half-Heusler experimentally,[48] and may also have good thermoelectric performance. This is perhaps a consequence of the fact that most experimentally synthesized half-Heusler compounds lie close to the convex hull that governs phase stability.[49]

Here we study a set of 75 potential half-Heusler compounds that were predicted to be stable and were studied previously in the context of thermal conductivity.[20] Importantly, this set was previously studied, with emphasis on thermal conductivity as the key first screen. Emphasis on thermal conductivity is a traditional approach in thermoelectrics research, as emphasized in Slack's influential phonon-glass-electron-crystal concept[50,51] and much work in the field.[52–56]

However, when we use band structure as a first screen, and then do detailed calculations for the compounds with favorable band structure, we find additional compounds, not previously identified, with promising thermoelectric properties. This emphasizes the importance of band structure in determining thermoelectric performance, even in a set, such as half-Heuslers, where the thermal conductivity varies strongly from compound to compound.

II. METHODS

A. Search Strategy

Calculations of electronic structures using first principles methods are now routine. However, there are two important limitations that make high throughput computations for thermoelectrics challenging. The first is that for σ one requires an electronic relaxation time (τ) in addition to transport functions determined by the band structure.[57] The second is that detailed calculations of thermal conductivity, while now possible due to recent advances, remain expensive compared to electronic structure calculations.[58] Here we first use an electronic fitness function (EFF) to screen band structures.

This function includes both doping and temperature dependence, but is very easy to compute. This provides an initial screen. The basic idea of the EFF is to measure the extent to which a given band structure decouples the contrary dependence of σ and S. It is important to note that this EFF addresses a key challenge for the discovery of thermoelectric materials. It identifies materials with band structure features such as complex carrier pockets, multiple anisotropic carrier pockets, band convergence, and combinations of heavy and light bands in a doping and temperature dependent way that is amenable to high throughput calculations.

We then do further more detailed calculations for the materials that have high peak EFF. We use deformation potential theory to calculate the relaxation time and we directly calculate the lattice thermal conductivity by solving the linearized Boltzmann-Peierls equation using the ShengBTE package.[59] These are time consuming calculations, which are facilitated by the fact that we use the EFF as a first screen thus avoiding calculations for those materials with low EFF. In this study we illustrate this approach at 1000 K, which is an important temperature for applications that have access to high grade heat sources.

B. Structures

Half-Heusler compounds have general chemical formula ABC and crystallize in a cubic structure, space group F$\bar{4}$3m. This structure contains three interpenetrating fcc sublattices. A occupies 4c ($\frac{1}{4},\frac{1}{4},\frac{1}{4}$). B occupies 4a (0,0,0) and C occupies 4b ($\frac{1}{2},\frac{1}{2},\frac{1}{2}$). The B and C atoms form a NaCl rocksalt subunit, with half of the eight tetrahedral voids occupied by A atoms. Thus the 4c site is unique, while exchange of B and C in the 4a and 4b sites does not change the material. There are thus three distinct variants for the atoms ABC depending on which element is in the 4c site.[60] Here we use this ABC notation for chemical formulas rather than the standard IUPAC notation in order to reduce ambiguity.

In high throughput calculations, it is important to reduce ambiguity due to possible database errors.[61] We calculated all three structural possibilities, and use the lowest energy one. We also use phonon calculations to check whether the structures of the identified compounds are dynamically stable. We find that this is the case, consistent with the report of Carrete and co-workers.[20]

C. Density functional theory calculations

We started with 75 half-Heusler compounds from Ref. 20. We constructed the three unique half-Heusler structures, as discussed above, for each composition. We optimized the lattice parameter for each using the projector augmented wave (PAW) method[62] as implemented in the Vienna Ab Initio Simulation Package (VASP), and selected the lowest energy ordering.[63] We used the Perdew-Burke-Ernzerhof generalized gradient approximation (PBE-GGA) in these calculations.[64] A 500 eV

cutoff energy and Brillouin zone sampling by 10×10×10 uniform **k**-point meshes were adopted.

The electronic structures of these 75 compounds were then calculated with the all-electron general potential linearized augmented plane-wave (LAPW) method,[65] as implemented in WIEN2k code.[66] We reoptimized the lattice parameters with this method, although no significant differences from the PAW results were found. The electronic structures for the transport calculations underlying the EFF were done using the modified Becke-Johnson (mBJ) potential.[67] This potential provides band gaps generally in better agreement with experiment than standard GGA functionals.[67–70] This is important for the study of thermoelectric materials. We note also that band dispersions play a key role in transport calculations. Kim and coworkers,[69] compared mBJ calculations with experiment for the band masses of five zinc blende semiconductors. They found that while mBJ generally improves the band masses relative to PBE-GGA, significant errors remain, with a general trend of overestimation of masses relative to experiment. This implies that future work will benefit if better approximations, amenable to high throughput, which specifically improve band dispersions and at the same time allow practical calculations on dense **k**-point grids, become available.

Spin-orbit coupling (SOC) was included in these calculations. We used a basis set cut-off parameter, $R_{MT}K_{max}$=9, where R_{MT} is the LAPW sphere radius and K_{max} is the planewave sector cutoff. The electronic transport parameters were obtained using the BoltzTraP code[57], based on first principles electronic structure data on a 32×32×32 **k**-point mesh in the Brillouin zone (BZ). The thermoelectric electronic fitness functions (EFF) were obtained using the transM code.[36]

D. Electrical transport properties

The electronic fitness function (EFF) is

$$t = \left(\frac{\sigma}{\tau}\right) S^2/N^{2/3}, \tag{1}$$

where σ is the electrical conductivity, τ is the carrier relaxation time, S is the Seebeck coefficient, and N is the electronic density of states per unit volume.[36] It measures the electronic structure related decoupling of σ and S for thermoelectric materials. As mentioned, it is a function of temperature and carrier concentration. Importantly, both S and σ/τ can be calculated directly using the BoltzTraP code,[57] making this fitness function well suited for application in high throughput screening.[38]

We note that the EFF differs considerably from the commonly applied uniform relaxation time approximation, where some fixed relaxation time is assumed. In particular, the EFF is used for the numerator of ZT and therefore has an implicit $1/T$ dependence of the relaxation time, as in the degenerate electron-phonon scattering model. This reduces the tendency of the uniform relaxation time to predict overly strong increases of ZT at high temperature. More significantly for the present work, it incorporates a density of states factor that reduces the EFF for high density of states.

The density of states dependence introduces an additional energy dependence (and therefore doping level dependence as well). This also implies a momentum dependence since momentum and energy are connected through the band dispersion. It is additionally notable that this density of states factor in the denominator of the EFF is sublinear with a 2/3 power, which differs from the linear dependence of the electron phonon coupling strength λ on density of states that is often seen in metals.[71] A consequence is that the EFF does favor band structures with multiple carrier pockets. This can be rationalized by the idea that high momentum scattering may often be weaker than low momentum scattering.

This density of states factor eliminates the tendency of the uniform relaxation time to predict that heavy mass parabolic band systems are the best, and the heavier, the better. It also means that the relaxation time decreases with carrier concentration. This brings the peak of the EFF with respect to doping level much closer to the actual optimum doping levels for thermoelectrics, and avoids spurious predictions of high ZT with low S. Here we used the EFF to screen the band structures of half-Heusler compounds, and then studied the electrical transport properties and the lattice thermal conductivity for the compounds with high EFF.

Following this screening, we used a deformation potential method to calculate electrical transport properties. These electrical transport properties were calculated using the BoltzTraP code[57] combined with the relaxation time obtained from a single parabolic band (SPB) model. This is an approximation, but is superior to the scaling $\tau^{-1} \propto TN^{2/3}$, which is implicit in the EFF applied in the initial screen. The result is an energy-dependent relaxation time, $\tau = \tau_0 E^r$, where τ_0 and r are constant for a given scattering mechanism. r =-1/2 for acoustic phonons,[72] which is thought to be the dominant scattering mechanism in good thermoelectric materials. This is based on the fact that near optimum doping the resistivity of good thermoelectrics generally increases with temperature, often roughly linearly in T, which is an electron phonon limited behavior for a degenerate semiconductor. This is commonly the case in half Heusler compounds with high ZT.[20,39–45]

The relaxation time for the acoustic phonon scattering is

$$\tau = \frac{2^{\frac{1}{2}}\pi\hbar^4\rho v_l^2}{3E_d^2\left(m^* k_B T\right)^{\frac{3}{2}}} \frac{F_0\left(\varepsilon\right)}{F_{\frac{1}{2}}\left(\varepsilon\right)} \tag{2}$$

where v_l is the longitudinal acoustic velocity, E_d is the deformation potential, m^* is the conductivity transport effective mass. $F_x\left(\varepsilon\right) = \int_0^\infty \frac{E^x}{1+\exp(E-\varepsilon)} dE$, $\varepsilon = \frac{E_F}{k_B T}$ is the reduced chemical potential. v_l can be obtained us-

ing $v_l = \sqrt{\frac{B+4/3G}{\rho}}$, and B and G are the bulk modulus and shear modulus, respectively. These can be evaluated from the elastic constants.[73] The elastic constants (C or C_{ij}) were calculated from the stress-strain relationship.[74] The transport effective mass, m^* can be written as $(m^*)^{-1} = \sigma/ne^2\tau$, and can be obtained directly as a function of temperature and doping level using BoltzTraP and transM. The deformation potential E_d is defined as $E_d = \Delta E/\left(\frac{\Delta V}{V}\right)$, The E_d for holes and electrons were calculated based on the energy changes of valence band maximum (VBM) and conduction band minimum (CBM) with volume change $\Delta V/V$.

E. Lattice thermal conductivity

The phonon dispersions and lattice thermal conductivity were obtained using 4×4×4 supercells (with 192 atoms in total). We found that smaller cells did not give uniformly converged results in this class of compounds. The phonon dispersions and the harmonic second order interatomic force constants (IFCs) were calculated using Phonopy.[75] The Grüneisen parameters, γ were calculated based on the volume dependence of the harmonic phonons, $\gamma_i = -\frac{V}{\omega_i}\frac{\partial\omega_i}{\partial V}$, with the volume is shrunk -2% and expanded +2%. We used the ShengBTE package[59] for the third-order force constants. All these calculations were based on underlying DFT calculations with VASP, as described above. A phonon momenta **q**-mesh of 15×15×15 was used in solving the transport equation for the thermal conductivities.

Within this method,[59] the lattice thermal conductivity κ_l is calculated as the sum of contributions over all the phonon modes λ with branch p and wave vector **q**:

$$\kappa_l \equiv \kappa_{\alpha\alpha} = \frac{1}{N_q V}\sum_{\lambda}\frac{\partial f}{\partial T}\left(\hbar\omega_\lambda\right)v_\lambda^\alpha v_\lambda^\alpha \tau_\lambda \qquad (3)$$

where N_q is the number of uniformly spaced **q** points in the BZ, V is the volume of the unit cell, f is the Bose-Einstein distribution function depending on the phonon frequency ω_λ, and v_λ^α is the phonon velocity. The phonon lifetime, τ_λ in the relaxation time approximation is the inverse of the total scattering rate. τ_λ is limited by the two-phonon scattering from isotopic disorder and three-phonon anharmonic scattering. Thus there is a sum a two-phonon isotopic scattering rate $1/\tau^{iso}$ and a three-phonon anharmonic scattering rate $1/\tau^{anh}$. $1/\tau^{anh}$ involves the sum over three-phonon transition probabilities $\Gamma^{\pm}_{\lambda\lambda'\lambda''}$, which can be calculated as:

$$\Gamma^{\pm}_{\lambda\lambda'\lambda''} = \frac{\hbar\pi}{8N}\left\{\begin{array}{c} 2\left(f_{\lambda'} - f_{\lambda''}\right) \\ f_{\lambda'} + f_{\lambda''} + 1 \end{array}\right\}\frac{\delta(\omega_\lambda \pm \omega_{\lambda'} - \omega_{\lambda''})}{\omega_\lambda\omega_{\lambda'}\omega_{\lambda''}}\left|V^{\pm}_{\lambda\lambda'\lambda''}\right|^2, \quad (4)$$

where the upper (lower) row is curly brackets go with the +(-) sign for absorption (emission) processes. The scattering matrix elements $V_{\lambda\lambda'\lambda''}$ depend on the third-order IFCs. The three-phonon scattering phase space, $\mathrm{W}^{\pm}_{\lambda}$ provides information on the contribution of phonon modes to the anharmonic scattering rates, which is defined as the sum of frequency-containing factors in the expression of $\Gamma^{\pm}_{\lambda\lambda'\lambda''}$,[76–78]

$$\mathrm{W}^{\pm}_{\lambda} = \frac{\hbar\pi}{8N}\sum_{\lambda' p''}\left\{\begin{array}{c} 2\left(f_{\lambda'} - f_{\lambda''}\right) \\ f_{\lambda'} + f_{\lambda''} + 1 \end{array}\right\}\frac{\delta(\omega_\lambda \pm \omega_{\lambda'} - \omega_{\lambda''})}{\omega_\lambda\omega_{\lambda'}\omega_{\lambda''}} \quad (5)$$

for absorption (+) and emission (-) processes. Thus there are three main ingredients for understanding the thermal conductivity, (1) the phonon group velocities, (2) the scattering phase space, which is determined by the phonon dispersions and (3) the anharmonic couplings.

Finally, it should be noted that the Boltzmann theory has limitations. Most importantly, it is not valid for very strong scattering, where the phonon mean free path would be shorter than a reasonable size of a wavepacket (e.g. the wavelength). This is equivalent to the Ioffe-Regel criterion for electronic scattering, and leads to the concept of a minimum thermal conductivity. Above the Debye temperature (Θ_D), κ_l decreases as $1/T$ when scattering is limited by Umklapp phonon scattering, until the minimum lattice thermal conductivity is reached. At this point the thermal conductivity becomes approximately constant, and may even increase with temperature due to transport involving non-propagating modes.[79] There is more than one expression for the minimum thermal conductivity in literature, but a commonly used one, which we use here is,[80,81]

$$\kappa_{min} = \left(\tfrac{\pi}{6}\right)^{\frac{1}{3}} k_B V^{-\frac{2}{3}}\sum_i v_i\left(\frac{T}{\Theta_i}\right)^2\int_0^{\Theta_i/T}\frac{x^3 e^x}{(e^x-1)^2}dx \quad (6)$$

where k_B is the Boltzmann constant, V is the average volume per atom, the sum is over three vibrational modes (two shear v_s and one longitudinal v_l), and $\Theta_i = v_i\left(\hbar/k_B\right)\left(6\pi^2/V\right)^{1/3}$. At high temperature ($\Gamma \gg \Theta_D$), one obtains $\kappa_{\min} = \frac{1}{2}\left(\frac{\pi}{6}\right)^{\frac{1}{3}} k_B V^{-\frac{2}{3}}\left(2v_s + v_l\right)$, where $v_s = \sqrt{\frac{G}{\rho}}$, $v_l = \sqrt{\frac{B+4/3G}{\rho}}$. $\Theta_D = v_m\left(\hbar/k_B\right)\left(6\pi^2/V\right)^{1/3}$, where $v_m = \left[\frac{1}{3}\left(\frac{1}{v_l^3} + \frac{2}{v_s^3}\right)\right]^{-\frac{1}{3}}$. Here we use the greater of the calculated thermal conductivity from ShengBTE and the minimum thermal conductivity from this formula to obtain ZT. This only applied to a single material, SiAlLi, for which we obtained a calculated κ_l=0.38 W/mK at 1000 K from ShengBTE. The minimum thermal conductivity for this material was 1.54 W/mK. It is also possible to estimate a different thermal conductivity limit by the small grain size limit, which is implemented in ShengBTE. In this approach phonon mean-free paths are controlled by an assumed small grain size. The result for SiAlLi is 2.1 W/mK.

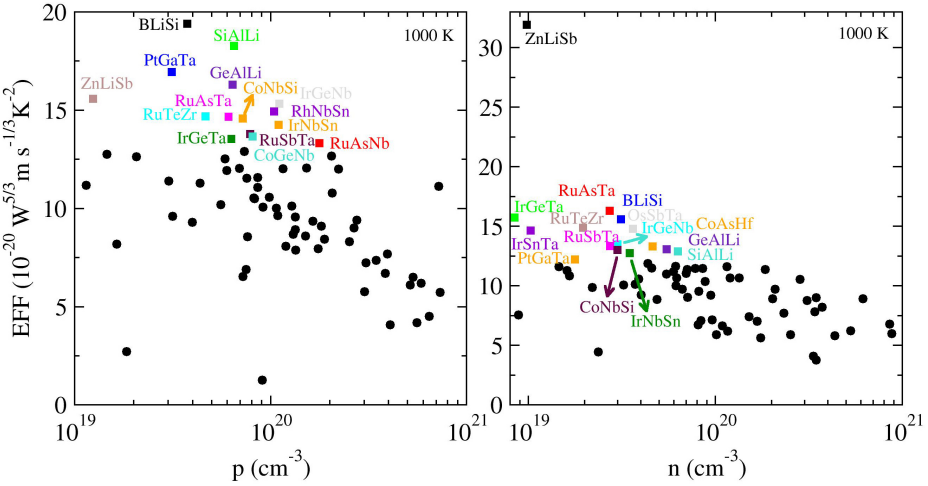

FIG. 1. Peak EFF and corresponding carrier concentration for the 74 half-Heusler compounds. The calculations are for 1000 K, and are shown for p-type (left) and n-type (right).

III. RESULTS AND DISCUSSION

A. Fast Electronic Structure Screening

As mentioned, we use a metric of the favorability of the electronic structure (the EFF) as a first screen. We calculated the electronic structures and the needed transport coefficients for the set of 75 half-Heusler compounds using the mBJ potential including SOC. We found that NiGaNb is does not have a band gap, and therefore is unsuitable as a high performance thermoelectric. In the following, we focus on the remaining 74 compounds. For the purpose of this work we also focus on a temperature of 1000 K. As mentioned, this is a temperature relevant to applications. It is also a temperature where half-Heusler compounds often show good performance.

We begin with the EFF. Fig. 1 shows the maximum EFF values and corresponding carrier concentrations for both p-type and n-type doping at 1000 K. We selected the 15 best materials for p-type and n-type based on the maximum EFF. These are the individually labeled compounds in the figure. The values of maximum EFF and corresponding doping carrier concentration are listed in Table I.

We briefly discuss the highest EFF compounds before proceeding to the remaining steps of our screening. The best materials from the point of view of EFF are BLiSi and ZnLiSb for p-type and n-type, respectively. These have peak EFF values of 1.94×10^{-19} $W^{5/3}ms^{-1/3}K^{-2}$ and 3.19×10^{-19} $W^{5/3}ms^{-1/3}K^{-2}$ at carrier concentration 3.76×10^{19} cm^{-3} and 9.8×10^{18} cm^{-3}, respectively.

The hexagonal polytype of LiZnSb (standard notation rather than the ABC notation for the half-Heusler structure) had been previously predicted to be an excellent thermoelectric,[18] while the cubic polytype was synthesized and studied more recently. It was predicted to be a good thermoelectric for both p-type and n-type.[82] Our EFF calculation suggests that the performance for n-type will be substantially better than for p-type at least at a temperature of 1000 K.

Turning to BLiSi, we observe that, although it is not the material with the highest n-type EFF, it does have a high n-type value of 1.56×10^{-19} $W^{5/3}ms^{-1/3}K^{-2}$. This is a relatively unstudied material. Moreover, its band gap of ∼0.6 eV and chemistry suggest that it may be a compound that could have stability and excellent thermoelectric performance at high temperatures, perhaps well above 1000 K. This would be interesting in topping cycle applications, for example. However, the fact that it is a light element compound with a dense structure suggests that it may be inferior to other materials from the point of view of thermal conductivity (see below).

As mentioned, thermoelectric properties are sensitive to the band structure. While the mBJ potential generally improves upon standard density functionals such as the PBE-GGA, there can be errors in the effective masses.[69] Accordingly, we also did band structure calculations with the HSE hybrid functional for this compound. These results (Supplemtary Information, Fig. 1) for BLiSi are very similar to the mBJ band structure, lending support to the mBJ results for this compound.

The band structure and carrier pocket visualizations of BLiSi are given in Fig. 2. The valence band maximum of BLiSi is at Γ and consists of a degenerate heavy hole and light hole band plus a spin-orbit split-off hole band. Due to the light elements, the spin orbit splitting is low and the split-off band is only 0.03 eV below the VBM, yielding an effective degeneracy of three. These have a mixture of heavy and light character with very strong pocket anisotropy due to **k** dependent interactions among these bands away from Γ. This very strong

TABLE I. Calculated maximum EFF (10^{-19} $W^{5/3}ms^{-1/3}K^{-2}$) and corresponding carrier concentration ($10^{19}cm^{-3}$), Seebeck coefficient (μV/K), and band gap (eV) for the 15 highest EFF thermoelectric candidates for p-type and n-type.

p-type compounds	maximum EFF	p	S	band gap	n-type compounds	maximum EFF	n	S	band gap
BLiSi	1.94	3.76	356	0.64	ZnLiSb	3.19	0.98	-439	0.84
SiAlLi	1.83	6.51	300	0.49	RuAsTa	1.63	2.72	-377	0.81
PtGaTa	1.69	3.13	447	0.86	IrGeTa	1.57	0.84	-426	1.05
GeAlLi	1.63	6.39	287	0.45	BLiSi	1.56	3.13	-306	0.64
ZnLiSb	1.56	1.24	396	0.84	RuTeZr	1.49	1.96	-500	1.23
IrGeNb	1.53	11.09	426	0.71	OsSbTa	1.48	3.63	-333	0.68
RhNbSn	1.49	10.41	398	0.64	IrSnTa	1.47	1.03	-419	1.03
RuTeZr	1.47	4.65	509	1.23	IrGeNb	1.35	2.99	-301	0.71
RuAsTa	1.47	6.10	440	0.81	RuSbTa	1.33	2.74	-345	0.77
CoNbSi	1.46	7.22	446	0.77	CoAsHf	1.33	4.61	-498	1.27
IrNbSn	1.42	10.97	421	0.67	GeAlLi	1.31	5.50	-253	0.45
RuSbTa	1.38	7.87	433	0.77	CoNbSi	1.30	3.00	-363	0.77
CoGeNb	1.37	8.11	485	1.00	SiAlLi	1.29	6.31	-250	0.49
IrGeTa	1.35	6.31	495	1.05	IrNbSn	1.27	3.49	-302	0.67
RuAsNb	1.33	17.75	334	0.52	PtGaTa	1.22	1.77	-370	0.86

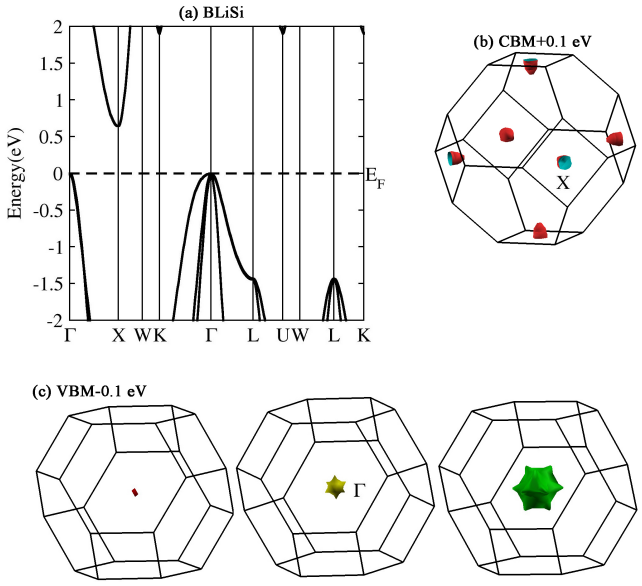

FIG. 2. Calculated (a) band structure including spin-orbit (b) electron carrier pocket visualization by constant energy surfaces 0.1 eV above the conduction band minimum, and (c) hole carrier pocket visualization by energy isosurfaces 0.1 eV below the valence band maximum for BLiSi.

anisotropy is evident from the band structure, where a heavy-light mixture of bands is seen along $\Gamma - K$ but not along $\Gamma - L$. It is also evident in the carrier pocket visualization, where carrier pockets very different from spheres are seen. This underlies the high p-type EFF. The conduction band minimum is at X, which yields a three-fold pocket degeneracy, and importantly, the pockets are quite anisotropic, which is a characteristic that favors high EFF.[37]

The electronic thermal conductivity is often written as $\kappa_e = L\sigma T$, where the standard value of the Lorenz number is L=2.45×10^{-8} WΩ/K^2. This is an approximation for thermoelectric materials, where it is often the case the the electronic thermal conductivity is somewhat lower than this value, although it can be higher if there is bipolar conduction.[83] In any case, with this expression, $ZT = \gamma S^2/L$, where $\gamma = \kappa_e/(\kappa_e + \kappa_l) \leq 1$ and κ_l is the lattice thermal conductivity. In this case, even assuming that lattice thermal conductivity is nil (γ=1), a minimum Seebeck coefficient of 156 μV/K is needed in order to achieve $ZT = 1$. It is a fact that high-performance thermoelectrics generally have high Seebeck coefficients larger than 200 μV/K as used. Therefore, besides EFF it is useful to screen out any compounds that have low Seebeck coefficient.

Fig. 3 shows the maximum EFF and the Seebeck coefficient at 1000 K for the doping level corresponding to the peak EFF. As seen, some of the compounds do have magnitudes of S lower than 200 μV/K, but these are not the high EFF compounds. Therefore we proceed to further screens for the high EFF compounds.

B. Lattice Thermal Conductivity

We calculated the lattice thermal conductivity of the 15 highest EFF compounds. The result is plotted in Fig. 4 again at 1000 K. In the case of SiAlLi, the minimum lattice thermal conductivity κ_{min}=1.54 W/mK is higher than the value obtained from the Boltzmann transport calculation with ShengBTE. Accordingly, we show the value of κ_{min} for this compound. Furthermore, as seen, there is a very large range, amounting to an order of magnitude, in κ_l for these compounds. Thus there is not a strong correlation between lattice thermal conductivity and peak EFF. Examples of high thermal conductivity materials include RuAsNb (11.2 W/mK) and IrSnTa (19.5 W/mK), both at 1000 K. Examples of low

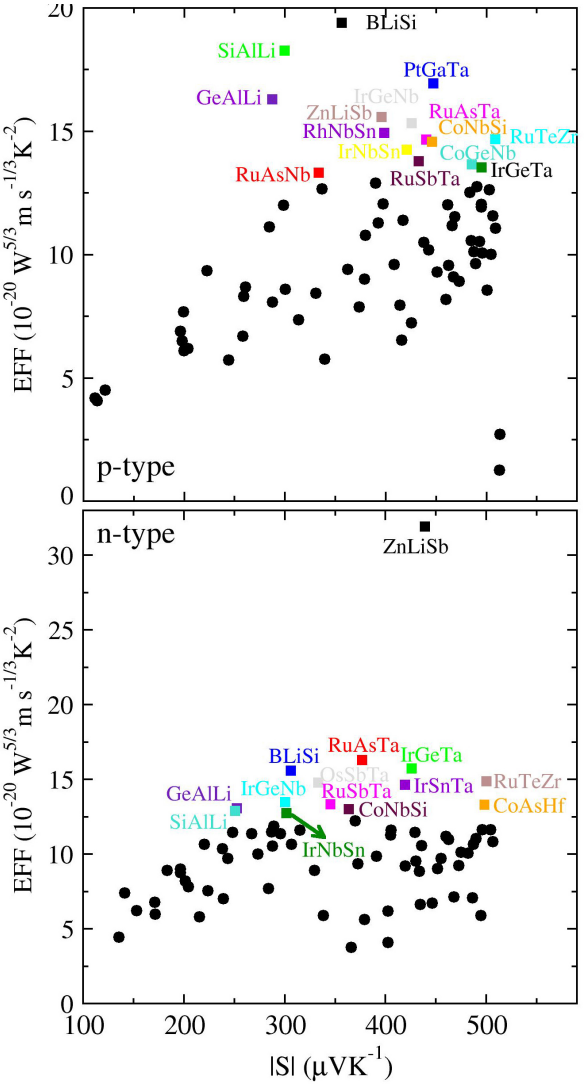

FIG. 3. Peak EFF and corresponding magnitude of the Seebeck coefficient at 1000 K for p-type and n-type.

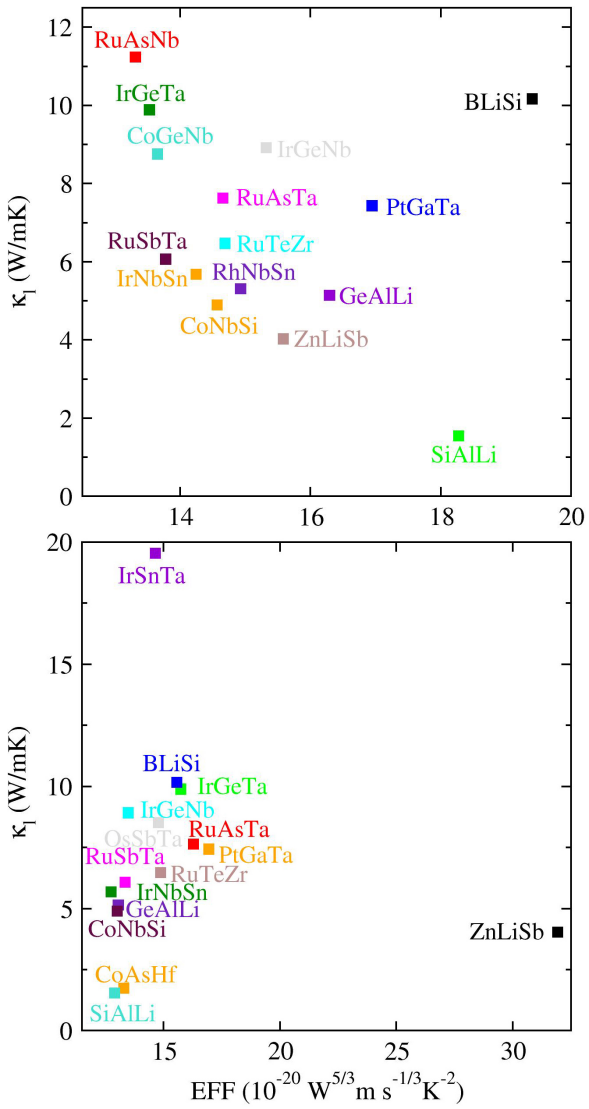

FIG. 4. Calculated lattice thermal conductivity and peak EFF at 1000 K for 15 highest EFF p-type and n-type compounds (note that the lattice thermal conductivity is the same for p-type and n-type, but that the compounds shown differ).

thermal conductivities include SiAlLi, as mentioned, and CoAsHf (1.74 W/mK). CoAsHf (conventionally written HfCoAs) is a previously identified good thermoelectric material.[21] Returning to the issue of polymorphism it was also predicted in a different structure type (orthorhombic $Pnma$).[46]

In any case, besides the large range in thermal conductivities in half-Heusler compounds, there is also considerable variation in phonon dispersions. The calculated phonon dispersion curves and the (projected) phonon density of states (PHDOS) of SiAlLi, CoAsHf and BLiSi are shown in Fig. 5. The calculated thermal conductivity of BLiSi, which as mentioned is a high EFF compound, is shown in Fig. 6.

The transverse and longitudinal acoustic branches in SiAlLi are relatively more separated than in BLiSi or CoAsHf. This separation is generally a reflection of more ionic structures and in particular less directional covalent bonding. This less direction bonding leads to softer shear modes relative to the longitudinal acoustic branch. It is also a feature that favors larger scattering phase space, and thus everything else being equal, lower thermal conductivity.

We note that the Grüneisen parameters for the low energy acoustic modes in SiAlLi are negative, in contrast to the normal positive values for the other two compounds. Negative Grüneisen parameters indicate nearness to a structural instability under pressure. It is also interesting to note that there are low frequency phonon modes around the L point of SiAlLi that are not present in the other two compounds.

It is also seen that in all three compounds the longitudinal acoustic branch intersects optical branches before

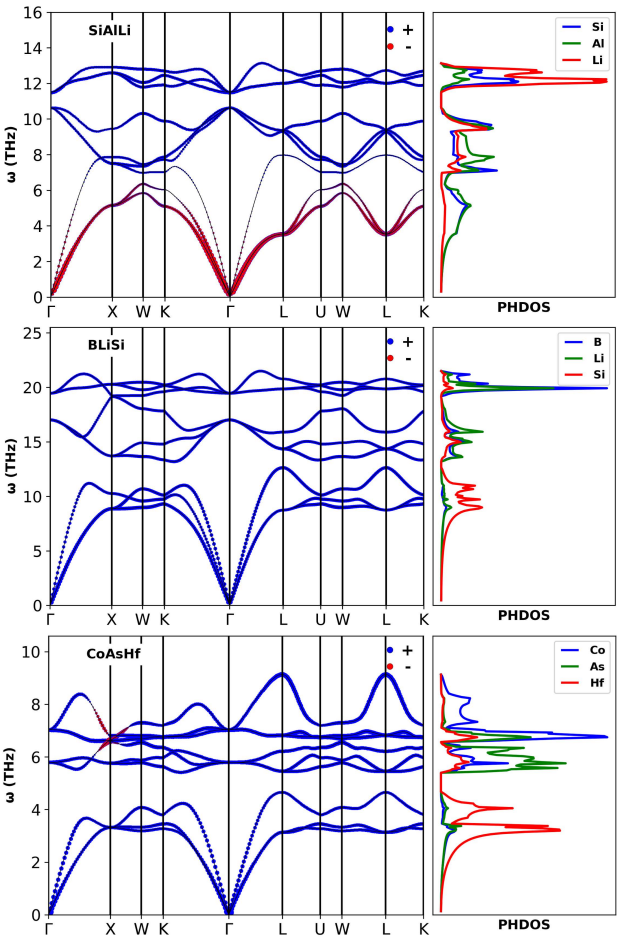

FIG. 5. Phonon dispersions and phonon density of states for SiAlLi (top) and BLiSi (middle) and CoAsHf (bottom). The point size denotes the Grüneisen parameter for the modes, with blue being positive (normal) and red indicating negative. Note the different frequency scales for the different compounds.

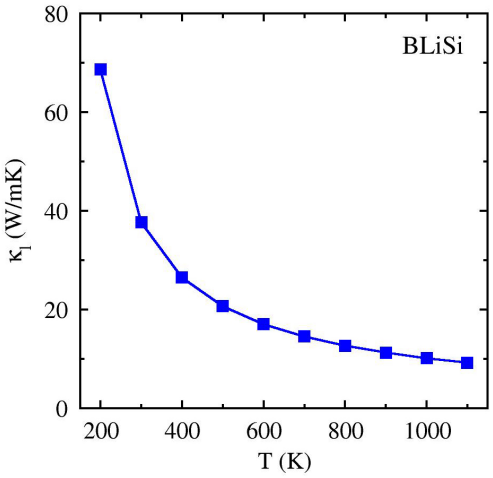

FIG. 6. Temperature dependent lattice thermal conductivity of BLiSi.

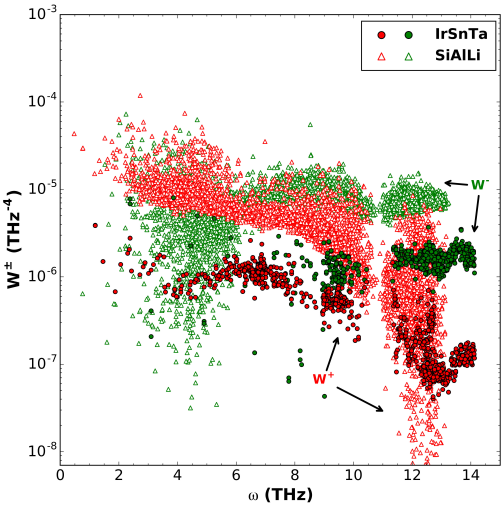

FIG. 7. Scattering phase space for different modes in very low thermal conductivity SiAlLi and high thermal conductivity IrSnTa. Note the log scale.

reaching the zone boundary. This intersection is expected to reduce the thermal conductivity since the longitudinal acoustic branch is normally the most important heat carrying phonon branch. In CoAsHf the effect of this intersection is strong enough to open a gap in the phonon spectrum from $\sim 4.5 - 5.5$ THz. It is also important to note the energy scales. BLiSi has much higher frequency phonons that the other two materials shown, and CoAsHf has a much lower energy scale than SiAlLi. Based on this consideration one would expect the thermal conductivities to be ordered CoAsHf < SiAlLi < BLiSi, which is not in fact the case for the first two compounds. This underscores the fact that the details are important, and simple rules based on lattice stiffness or sound velocity, while useful, are not sufficient. In the case of BLiSi, the thermal conductivity is relatively high at 1000 K. Depending on its chemical stability its best performance may be at higher temperature.

The calculated three-phonon anharmonic scattering phase space for SiAlLi is shown in Fig. 7, where it are compared with the high thermal conductivity material IrSnTa. The clear difference for the thermal conductivity is in the scattering phase space. Specifically, the scattering phase space for SiAlLi is higher by an order of magnitude or more than that of IrSnTa. Thus even though it is composed of light elements, SiAlLi can have a much lower lattice thermal conductivity than IrSnTa.

C. Electronic Transport

The electrical transport properties were calculated using the BoltzTraP code[57] combined with the relaxation time obtained from deformation potential theory.[72] This is the last step needed for evaluation of ZT. Transport

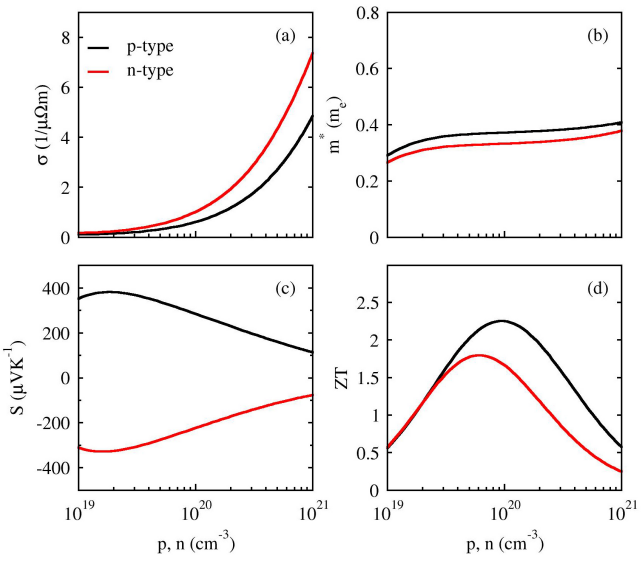

FIG. 8. Calculated electrical transport properties for BLiSi: (a) electrical conductivity, σ, (b) transport effective mass for conductivity, m^*, (c) Seebeck coefficient, S, and (d) ZT as a function of carrier concentration at 1000 K.

coefficients for BLiSi are given in Fig. 8, showing both p-type and n-type. The calculated peak ZT values at the optimal doping and the corresponding carrier concentrations are shown in Fig. 9. Several compounds show calculated maximum ZT of near or above 1.5 at 1000 K. These include SiAlLi, BLiSi, PtGaTa, GeAlLi, CoNbSi, IrNbSn for p-type and CoAsHf, ZnLiSb, BLiSi, SiAlLi, GeAlLi for n-type.

SiAlLi and GeAlLi have also been previously synthesized and their thermoelectric properties investigated.[84,85] Very high ZT was not found experimentally. However, the present results in combination with the existing experimental data suggest further investigation and optimization of those compounds. CoNbSi has also been studied previously.[46] It should be noted that some of the identified compounds contain expensive components, including Ge and especially Ir and Pt. This would restrict their use in applications. As mentioned, CoAsHf and ZnLiSb were identified as potential high ZT in previous theoretical studies,[21,82] consistent with what is found here. BLiSi and PtGaTa are candidates identified here.

Importantly, BLiSi is not a very low thermal conductivity material, and therefore might not have been identified if we had screened first based on thermal conductivity. We discuss this material in more detail below. We note n-type BLiSi has higher electrical conductivity than p-type. This is due to the lighter transport effective mass, as seen in Fig. 8(b), and the different scattering rate. Correspondingly, the magnitude of S is somewhat higher for p-type, reflecting the usual opposite behavior in S and σ. However, the EFF is high for both p-type and n-type. As mentioned above, this is due to carrier

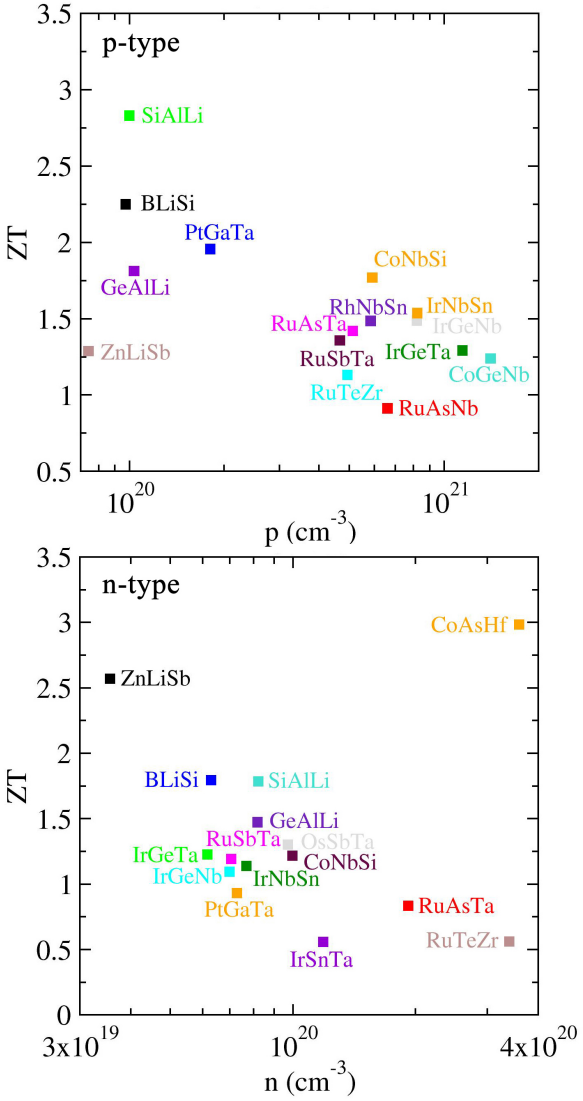

FIG. 9. Calculated optimized ZT at 1000 K for the high EFF p-type and n-type compounds.

pocket degeneracy, heavy-light band mixtures for p-type and carrier pocket anisotropy. Finally, the ZT is higher for p-type than for n-type, consistent with the trend in the EFF.

The maximum ZT for p-type BLiSi is ~2.2 at carrier concentration of $\sim 10^{20}$ cm^{-3}. A value of $ZT \sim 1.8$ at $\sim 6\times10^{19}$ cm^{-3} is obtained for n-type. Both of these values are at 1000 K.

We note that these high values of ZT depend on achieving suitable doping levels, while maintaining high mobility. In the case of BLiSi, the chemical formula suggests a Zintl type of bonding, specifically, Li cations donating charge to form a bonding eight valence electron $(BSi)^-$ anionic framework. This is consistent with the electronic structure. In such compounds the cation may be relatively weakly bonded and is not active in the electronic structure near the band edges, thus providing an

opportunity for doping. We did defect calculations for a number of possible neutral defects. Details and defect formation energies are given in Supplementary Information Table I. Consistent with the expectation discussed above, we find that the lowest energy defect is the Li vacancy. The Li vacancy formation energy is 0.89 eV. We also find from the electronic structure (Supplementary Fig. 2), that Li vacancies are p-type dopants. A potential n-type dopant may be Mg on the Li site.

The second question is whether this would lead to reasonable mobility. From the density of states one observes that Li vacancies do not strongly distort the band edges, which is a favorable indication. It is also to be noted that dopants imply ionized impurities, which then may result in ionized impurity scattering to the detriment of the mobility. However, this can be avoided by screening.[86] According to the Brooks-Herring formula the ionized impurity limited mobility is approximately proportional to the square of the dielectric constant. The calculated dielectric constant for BLiSi, as obtained with the PBE-GGA and VASP, is 13.9, which is reasonable for good semiconducting behavior but not very high. For comparison the dielectric constant of Si is 11.7. The other identified good thermoelectric compounds have higher values of 25.5, 33.8 and 18.1, for CoAsHf, CoNbSi and SiAlLi, respectively. It will be of interest to experimentally investigate doping in BLiSi and determine the extent to which high carrier concentrations can be achieved while maintaining suitable mobility.

While our calculations include a number of approximations, they do suggest experimental investigation of the thermoelectric properties of BLiSi in half-Heusler structure at 1000 K and above.

IV. CONCLUSIONS

We discuss and demonstrate a strategy for high-throughput identification of new half-Heusler compounds that uses a fast metric based on electronic structure as a first screen. This leads to the identification of several previously identified materials. Importantly, it also leads to identification of additional compounds as promising thermoelectrics. The fact that previously unidentified promising compounds are found within a previously studied set emphasizes the importance of electronic structure, and in particular the decoupling of σ and S, measured by the EFF, in thermoelectric performance. We started with 75 half-Heusler compounds, and first screened their band structures using a readily calculated electronic fitness function that focuses on decoupling of S and σ by band structure features. More detailed calculations of thermal conductivity and electronic transport were then performed for the compounds with highest EFF. Compounds identified in this way include BLiSi and PtGaTa. BLiSi may be particularly interesting as a high temperature thermoelectric material.

ACKNOWLEDGMENTS

Work at the University of Missouri was supported by the U.S. Department of Energy, Office of Science, Basic Energy Sciences, Award Number DE-SC0019114. Work at ISSP and USTC was supported by National Science Foundation of China, Award Number 11774347. Z.F. gratefully acknowledges support from the China Scholarship Council (CSC).

* yshzhang@theory.issp.ac.cn
† singhdj@missouri.edu
‡ yshzhang@theory.issp.ac.cn; singhdj@missouri.edu

[1] C. Wood, Rep. Prog. Phys. **51**, 459 (1988).
[2] J. Yang and T. Caillat, MRS Bull. **31**, 224 (2006).
[3] L. E. Bell, Science **321**, 1457 (2008).
[4] J. Yang, L. Xi, W. Qiu, L. Wu, X. Shi, L. Chen, J. Yang, W. Zhang, C. Uher, and D. J. Singh, NPJ Comput. Mater. **2**, 15015 (2016).
[5] J. He and T. M. Tritt, Science **357**, eaak9997 (2017).
[6] H. Zhang, C. X. Liu, X. L. Qi, X. Dai, Z. Fang, and S. C. Zhang, Nat. Phys. **5**, 438 (2009).
[7] L. Muchler, F. Casper, B. Yan, S. Chadov, and C. Felser, Phys. Stat. Sol. RRL **7**, 91 (2012).
[8] H. Shi, D. Parker, M. H. Du, and D. J. Singh, Phys. Rev. Appl. **3**, 014004 (2015).
[9] S. Mashhadi, D. L. Duong, M. Burghard, and K. Kern, Nano Lett. **17**, 214 (2017).
[10] I. Terasaki, Y. Sasago, and K. Uchinokura, Phys. Rev. B **56**, R12685 (1997).
[11] K. Izawa, K. Behnia, Y. Matsuda, H. Shishido, R. Settai, Y. Onuki, and J. Flouquet, Phys. Rev. Lett. **99**, 147005 (2007).
[12] T. Takabatake, E. Matsuoka, S. Narazu, K. Hayashi, S. Morimoto, T. Sasakawa, K. Umeo, and M. Sera, Physica B **383**, 93 (2006).
[13] G. Xing, X. Fan, W. Zheng, Y. Ma, H. Shi, and D. J. Singh, Sci. Rep. **5**, 10782 (2015).
[14] P. B. Allen and M. L. Cohen, Phys. Rev. **177**, 704 (1969).
[15] J. Goldak, C. S. Barrett, D. Innes, and W. Youdelis, J. Chem. Phys. **44**, 3323 (1966).
[16] H. Zhu and C. Xiao, Front. Phys. **13**, 138112 (2018).
[17] J. Sun, J. Shuai, Z. Ren, and D. J. Singh, Mater. Today Phys. **2**, 40 (2017).
[18] G. K. H. Madsen, J. Am. Chem. Soc. **128**, 12140 (2006).
[19] C. Barreteau, J.-C. Crivello, J.-M. Joubert, and E. Alleno, Comput. Mater. Sci. **156**, 96 (2019).
[20] J. Carrete, W. Li, N. Mingo, S. Wang, and S. Curtarolo, Phys. Rev. X **4**, 011019 (2014).
[21] S. Bhattacharya and G. K. H. Madsen, J. Mater. Chem. C **4**, 11261 (2016).
[22] R. Li, X. Li, L. Xi, J. Yang, D. J. Singh, and W. Zhang, ACS Appl. Mater. Interfaces **11**, 24859 (2019).
[23] A. F. Ioffe, *Semiconductor thermoelements and thermoelectric cooling* (Infosearch, London, 1957).

[24] X. Chen, D. Parker, and D. J. Singh, Sci. Rep. **3**, 3168 (2013).
[25] Y. Pei, X. Shi, A. LaLonde, H. Wang, L. Chen, and G. J. Snyder, Nature **473**, 66 (2011).
[26] J. Sun and D. J. Singh, J. Mater. Chem. A **5**, 8499 (2017).
[27] H. Shi, W. Ming, D. S. Parker, M.-H. Du, and D. J. Singh, Phys. Rev. B **95**, 195207 (2017).
[28] J. Sun and D. J. Singh, Phys. Rev. Appl. **5**, 024006 (2016).
[29] D. S. Parker, A. F. May, and D. J. Singh, Phys. Rev. Appl. **3**, 064003 (2015).
[30] N. A. Mecholsky, L. Resca, I. L. Pegg, and M. Fornari, Phys. Rev. B **89**, 155131 (2014).
[31] G. Xing, J. Sun, K. P. Ong, X. Fan, W. Zheng, and D. J. Singh, APL Mater. **4**, 053201 (2016).
[32] H. Usui and K. Kuroki, J. Appl. Phys. **121**, 165101 (2017).
[33] Devender, P. Gehring, A. Gaul, A. Hoyer, K. Vakilnova, R. J. Mehta, M. Burghard, T. Borca-Tascuic, D. J. Singh, K. Kern, and G. Ramanath, Adv. Mater. **28**, 6436 (2016).
[34] D. Parker, X. Chen, and D. J. Singh, Phys. Rev. Lett. **110**, 146601 (2013).
[35] A. Jain, S. P. Ong, G. Hautier, W. Chen, W. D. Richards, S. Dacek, S. Cholia, D. Gunter, D. Skinner, G. Ceder, and K. A. Persson, APL Mater. **1**, 011002 (2013).
[36] G. Xing, J. Sun, Y. Li, X. Fan, W. Zheng, and D. J. Singh, Phys. Rev. Materials **1**, 065405 (2017), erratum, Phys. Rev. Materials **1**, 079901 (2017).
[37] G. Xing, J. Sun, Y. Li, X. Fan, W. Zheng, and D. J. Singh, J. Appl. Phys. **123**, 195105 (2018).
[38] L. Bassman, P. Rajak, R. K. Kalia, A. Nakano, F. Sha, J. Sun, D. J. Singh, M. Aykol, P. Huck, K. Persson, and P. Vashishta, npj Comput. Phys. **4**, 74 (2018).
[39] Q. Shen, L. Chen, T. Goto, T. Hirai, J. Yang, G. P. Meisner, and C. Uher, Appl. Phys. Lett. **79**, 4165 (2001).
[40] C. Fu, S. Bai, Y. Liu, Y. Tang, L. Chen, X. Zhao, and T. Zhu, Nature Comm. **6**, 8144 (2015).
[41] L. Huang, Q. Zhang, B. Yuan, X. Lai, X. Yan, and Z. Ren, Mater. Res. Bull. **76**, 107 (2016).
[42] J. Yu, K. Xia, X. Zhao, and T. Zhu, J. Phys. D: Appl. Phys. **51**, 113001 (2018).
[43] T. Zhu, Y. Liu, C. Fu, J. P. Heremans, J. G. Snyder, and X. Zhao, Adv. Mater. **29**, 1605884 (2017).
[44] D. Black, L. Schoensee, J. Richardson, T. Vleisides, N. Kempf, D. Wang, Z. Ren, and Y. Zhang, ACS Appl. Energy Mater. **1**, 5986 (2018).
[45] H. Zhu, J. Mao, Y. Li, J. Sun, Y. Wang, Q. Zhu, G. Li, Q. Song, J. Zhou, Y. Fu, R. He, T. Tong, Z. Liu, W. Ren, L. You, Z. Wang, J. Luo, A. Sotnikov, J. Bao, K. Nielsch, G. Chen, D. J. Singh, and Z. Ren, Nature Comm. **10**, 270 (2019).
[46] R. Gautier, X. Zhang, L. Hu, L. Yu, Y. Lin, T. O. L. Sunde, D. Chon, K. R. Poeppelmeier, and A. Zunger, Nature Chem. **7**, 308 (2015).
[47] A. Zakutayev, X. Zhang, A. Nagaraja, L. Yu, S. Lany, T. Mason, D. S. Ginley, and A. Zunger, J. Am. Chem. Soc. **135**, 10048 (2013).
[48] C. S. Lue, Y. Oner, D. G. Naugle, and J. H. Ross, IEEE Trans. Magn. **37**, 2138 (2001).
[49] J. Ma, V. I. Hegde, K. Munira, Y. Xie, S. Keshavarz, D. T. Mildebrath, C. Wolverton, A. W. Ghosh, and W. H. Butler, Phys. Rev. B **95**, 024411 (2017).
[50] G. A. Slack, MRS Symp. Proc. **478**, 47 (1997).
[51] G. S. Nolas, D. T. Morelli, and T. M. Tritt, Annu. Rev. Mater. Sci. **29**, 89 (1999).
[52] D. M. Rowe, V. S. Shukla, and N. Savvides, Nature **290**, 765 (1981).
[53] B. C. Sales, D. Mandrus, and R. K. Williams, Science **272**, 1325 (1996).
[54] V. Keppens, D. Mandrus, B. C. Sales, B. C. Chakoumakos, P. Dai, R. Coldea, M. B. Maple, D. A. Gajewski, E. J. Freeman, and S. Bennington, Nature **395**, 876 (1998).
[55] B. Poudel, Q. Hao, Y. Lan, A. Minnich, B. Yu, X. Yan, D. Wang, A. Muto, D. Vashaee, X. Chen, J. Liu, M. S. Dresselhaus, G. Chen, and Z. Ren, Science **320**, 634 (2008).
[56] C. Wan, Y. Wang, N. Wang, W. Norimatsu, M. Kusunoki, and K. Koumoto, Sci. Technol. Adv. Mater. **11**, 044306 (2010).
[57] G. K. H. Madsen and D. J. Singh, Comput. Phys. Commun. **175**, 67 (2006).
[58] L. Lindsay, C. Hua, X. L. Ruan, and S. Lee, Mater. Today Phys. **7**, 106 (2018).
[59] W. Li, J. Carrete, N. A. Katcho, and N. Mingo, Comput. Phys. Commun. **185**, 1747 (2014).
[60] D. Bende, Y. Grin, and F. R. Wagner, Chemistry **20**, 9702 (2014).
[61] A. Zunger, Nature **556**, 447 (2019).
[62] P. E. Blöchl, Phys. Rev. B **50**, 17953 (1994).
[63] G. Kresse and J. Furthmller, Comput. Mater. Sci. **6**, 15 (1996).
[64] J. P. Perdew, K. Burke, and M. Ernzerhof, Phys. Rev. Lett. **77**, 3865 (1996).
[65] D. J. Singh and L. Nordstrom, *Planewaves, Pseudopotentials, and the LAPW method, 2nd Ed.* (Springer, Berlin, 2006).
[66] K. Schwarz, P. Blaha, and G. K. H. Madsen, Comput. Phys. Commun. **147**, 71 (2002).
[67] F. Tran and P. Blaha, Phys. Rev. Lett. **102**, 226401 (2009).
[68] D. Koller, F. Tran, and P. Blaha, Phys. Rev. B **83**, 195134 (2011).
[69] Y. S. Kim, M. Marsman, G. Kresse, F. Tran, and P. Blaha, Phys. Rev. B **82**, 205212 (2010).
[70] D. J. Singh, Phys. Rev. B **82**, 205102 (2010).
[71] D. A. Papaconstantopoulos, W. E. Pickett, B. M. Klein, and L. L. Boyer, Nature **308**, 494 (1984).
[72] J. Bardeen and W. Shockley, Phys. Rev. **80**, 72 (1950).
[73] J. M. J. den Toonder, J. A. W. v. Dommelen, and F. P. T. Baaijens, Modell. Simul. Mater. Sci. Eng. **7**, 909 (1999).
[74] M. L. Kachanov, B. Shafiro, and I. Tsukrov, *Handbook of elasticity solutions* (Springer Science & Business Media, 2013).
[75] A. Togo, F. Oba, and I. Tanaka, Phys. Rev. B **78**, 134106 (2008).
[76] Y. Fu, D. J. Singh, W. Li, and L. Zhang, Phys. Rev. B **94**, 075122 (2016).
[77] A. Ward, D. A. Broido, D. A. Stewart, and G. Deinzer, Phys. Rev. B **80**, 125203 (2009).
[78] W. Li, L. Lindsay, D. A. Broido, D. A. Stewart, and N. Mingo, Phys. Rev. B **86**, 174307 (2012).
[79] M. Simoncelli, N. Marzari, and F. Mauri, Nature Physics (2019), doi:10.1038/s41567-019-0520-x.
[80] D. G. Cahill and R. O. Pohl, Annu. Rev. Phys. Chem. **39**, 93 (1988).
[81] D. G. Cahill, S. K. Watson, and R. O. Pohl, Phys. Rev. B **46**, 6131 (1992).
[82] M. A. White, G. J. Miller, and J. Vela, J. Am. Chem. Soc. **138**, 14574 (2016).

[83] A. Putatunda and D. J. Singh, Mater. Today Phys. **8**, 49 (2019).
[84] L. Spina, Y. Z. Jia, B. Ducourant, M. Tillard, and C. Belin, Zeitschrift für Kristallographie-Crystalline Materials **218**, 740 (2003).
[85] J. Barth, G. H. Fecher, M. Schwind, A. Beleanu, C. Felser, A. Shkabko, A. Weidenkaff, J. Hanss, A. Reller, and M. Kohne, J. Electron. Mater. **39**, 1856 (2010).
[86] X. He, D. J. Singh, P. Boon-on, M. W. Lee, and L. Zhang, J. Am. Chem. Soc. **140**, 18058 (2018).